JOURNAL OF MATERIALS SCIENCE 27 (1992) 2641–2648

Constant heating rate analysis of simultaneous sintering mechanisms in alumina

S. H. HILLMAN*, R. M. GERMAN†
Materials Engineering Department, Rensselaer Polytechnic Institute, Troy, NY 12180-3590, USA

Constant heating rate sintering experiments were conducted on a submicron alumina powder during the initial stage. Shrinkage was measured by precision dilatometry and surface area reduction was monitored with gas adsorption measurements. Furthermore, grain size and pore size results were collected using X-ray line broadening and mercury porosimetry. Analysis of the shrinkage and surface area reduction data showed excellent correlation with a computer simulation based on simultaneous surface diffusion and grain boundary diffusion mechanisms. A comparison of the simulated and the experimental sintering paths on a plot of surface area reduction versus shrinkage indicated the combination of mechanisms and activations energies which best describe this sintering behaviour. From this analysis the estimated activation energies for grain boundary and surface diffusion are 440 and 508 kJ mol^{-1}, respectively.

1. Introduction

Initial stage sintering kinetics have been investigated extensively, as summarized by Exner [1]. The early models of initial stage sintering involved several geometric approximations and ignored the possibility of multiple transport mechanisms. Quantitative descriptions of the contact between particles required simplifying approximations of the geometry, including the neck area, neck volume, radius of curvature, and distance over which diffusion occurs. These approximations are inaccurate compared with exact treatments that solve for the true neck shape. Alternatively, the geometrical changes during sintering have been treated using numerical techniques [2–9], many of which are subject to criticism [10, 11].

Isothermal studies have provided much of the sintering data in the past but there are substantial problems in reconciling the theory with experiment, especially those involving activation energy analyses [12]. Part of this problem originates from the finite time needed to heat a compact to the isothermal sintering temperature. Various corrections are applied to the sintering results to account for the transient events encountered during heating [13]. Although considerable past research has been performed on the initial sintering stage of alumina using isothermal data, there is controversy as to the importance of the various transport mechanisms. For example, past observations have concluded that alumina sinters by grain boundary diffusion [13–15], volume diffusion [16–18] and surface diffusion [19–23]. One possible explanation for these differing conclusions is that many researchers only conducted single measures of the sintering behaviour. The fundamental event is neck growth, which is accompanied by a significant reduction in compact surface area. If neck growth involves mass moving from sources on the particle surface (vapour transport or surface diffusion), then no shrinkage will occur during sintering. Alternatively, neck growth, surface area loss and shrinkage will all be observed if mass transport is from the interior of the particles. This occurs when grain boundary or volume diffusion takes place. Thus, sintering measured by a single monitor such as shrinkage will fail to observe the simultaneous effects of non-densification events. Furthermore, there are recognized changes in the rate of sintering and dominant mechanism with variations in temperature, heating rate, particle size, green density, agglomeration, atmosphere, and even the degree of sintering [24–31].

Two key decisions were made in the effort to minimize experimental errors. First, constant heating rate measurements were used to emphasize the initial portion of the process [32–35]. Such an approach is well suited to monitoring initial events and does not require time or temperature corrections for the heating portion of the cycle. Second, shrinkage and surface area were both measured to monitor the geometric changes and mechanisms of sintering. The use of these parallel measures provides an assessment of the sintering behaviour from two views. Shrinkage reflects the direct action of densification mechanisms like grain boundary diffusion; although simultaneous coarsening processes alter the driving force. In contrast, surface area reduction provides information on the total rate of neck growth by all sintering

Present address: Tegmen Corporation, 1153 West Fayette St., Syracuse, NY 13204, USA.
†*Present address*: Brush Chair in Materials, Engineering Science and Mechanics, Pennsylvania State University, 227 Hammond, University Park, PA 16802.

mechanisms. The interaction between mechanisms with respect to the experimental results were assessed via computer simulated behaviour.

2. Experimental procedure

A special high purity alpha-alumina powder with a small particle size was selected for these studies (the powder originally from Baikowski International Corporation, Charlotte, NC, was donated by K. Lay, GE Research and Development, Schenectady, NY). The powder was sintered in the as-received condition without sintering aids. The measured characteristics of the powder are outlined in Table I. The 0.14 μm particle size was determined by sizing in a scanning electron microscope (SEM). The powder is predominantly composed of mono-sized, rounded polycrystalline particles, with approximately 20 vol % of the particles consisting of small particle clusters. The BET specific surface area was 22.1 $m^2 g^{-1}$, giving an equivalent mean spherical particle diameter of 0.06 μm which is near the mean grain size of 0.044 μm, as measured by X-ray line broadening. For comparison, a laser technique was used to measure the particle size from Brownian motion, giving an agglomerate size of 0.66 μm. This later technique indicated that 85% of the particle clusters were below 1 μm. The differences between these measures of particle size are largely attributed to agglomeration. Optical emission spectroscopy was performed for chemical analysis, indicating that only silicon and tin were present at concentrations over 10 p.p.m. X-ray diffraction (XRD) analysis detected only α-alumina in the starting powder.

The powder was compacted in a floating die at a pressure of 33 MPa, giving a green density of 1.35 $g cm^{-3}$ which corresponds to 32% of the theoretical value for alumina. This pressure gave sound compacts without cracks or delamination on ejection. The compacts were approximately 12 mm in diameter and 6 mm in height. A thin coating of zinc stearate was used as a die wall lubricant in the compaction process.

TABLE I Powder characteristics

Mean particle size: 0.14 μm
Mean agglomerate size: 0.66 μm
Specific surface area: 22.1 $m^2 g^{-1}$
Mean X-ray grain size: 44 nm
Apparent density: 0.22 $g cm^{-3}$
Tap density: 0.41 $g cm^{-3}$
Pressed density: 1.35 $g cm^{-3}$
Chemical analysis (detected levels):
B < 10 p.p.m.
Ca ~ 10 p.p.m.
Cu ~ 10 p.p.m.
Fe ~ 10 p.p.m.
Ga ~ 10 p.p.m.
K ~ 10 p.p.m.
Li ~ 0.1 p.p.m.
Mg ~ 10 p.p.m.
Mo < 10 p.p.m.
Na ~ 10 p.p.m.
Pb ~ 1 p.p.m.
Si ~ 100 p.p.m.
Sn ~ 20 p.p.m.

The surface layer of lubricant was removed after pressing.

The green pellets were subjected to one of two different sintering tests. The first test started with determination of the surface area of each compact using nitrogen gas adsorption. Subsequently the compacts were sintered in an argon atmosphere at a constant heating rate of 5 K min^{-1}. Measurable compact changes started at approximately 1100 K, so at each 50 K interval ranging from 1123 to 1573 K (900–1300 °C), four compacts were removed from the heating process and air cooled. Cooling was sufficiently rapid that no time corrections were applied to the data. The surface area was measured to calculate the change for each compact due to heating. The surface area reduction ($\Delta S/S_0$) represents the magnitude of surface area change normalized to the initial surface area. The second test was performed using a precision, constant load dilatometer constructed from alumina. Contact between the alumina pushrod and compact was maintained by a 10 g weight on the pushrod, which was 3 mm in diameter. The compacts were heated at 5 K min^{-1} from room temperature to 1873 K in argon. Computer collected shrinkage and temperature data were accumulated constantly during the heating process. This experiment was repeated three times. The shrinkage ($\Delta L/L_0$) was determined from the dilatometer measured length change and initial compact size. Special effort was put into temperature calibration and control thermocouple location to ensure accurate readings. By the time detectable sintering took place, the heating rate was controlled within 0.1 K min^{-1}.

Mercury porosimetry was used to measure the pore size distribution of an initial compact, giving a median pore diameter of 118 nm. This technique was also applied to compacts heated at 5 K min^{-1} to 1223, 1423, and 1523 K. Likewise, X-ray line broadening was used to monitor grain coarsening during sintering. The diffraction peak at approximately 35° was profile analysed by curve fitting to determine the peak broadening at one half of the maximum intensity. A quartz standard was used to correct for the machine broadening, allowing determination of the grain size by the Scherrer formula [36]. Further compact characterization was performed using SEM, transmission electron microscopy (TEM), infrared spectroscopy (IRS), XRD, and electron paramagnetic resonance (EPR) to ensure that the observed changes were not due to defects, second phases, or other unanticipated causes.

3. Results

Fig. 1 provides a summary of the normalized shrinkage, surface area reduction, pore size and grain size results from the specimens heated to various temperatures. The error bars in the surface area reduction plot represent the standard deviation of the four replica samples. The dilatometer experiments were continued to 1873 K, with three replication runs. The shrinkage and shrinkage rate results are shown versus temperature in Figs 2 and 3. These illustrate the good

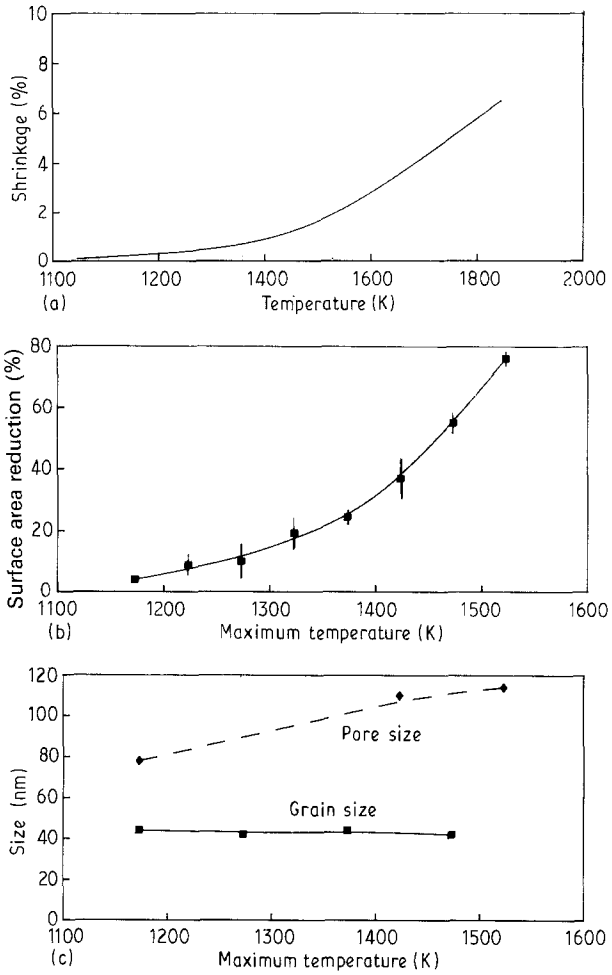

Figure 1 Plots of (a) shrinkage (b) surface area reduction, and (c) pore and grain size as functions of the maximum temperature during constant heating at 5 K min^{-1}.

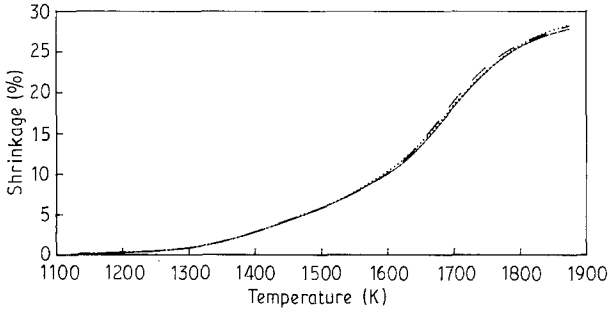

Figure 2 Shrinkage versus temperature as recorded by the dilatometer during heating at 5 K min^{-1} in three replication experiments.

reproducibility of the dilatometry results, both in terms of shrinkage and shrinkage rate. The shrinkage rate plot is not smooth but has relative peaks at approximately 1400, 1600 and 1700 K. The analysis by Wei [37] determined this was largely associated with agglomeration. To test for this possibility, the alumina powder was milled 24 h in a glass jar with alumina balls and subjected to the same constant heating dilatometry. Milling increased the initial surface area of the powder to 26.9 m^2 g^{-1} (compared with 22.1 m^2 g^{-1} for the unmilled powder). Chemical analysis indicated that milling did not drastically contaminate the powder, with only an increase in the boron

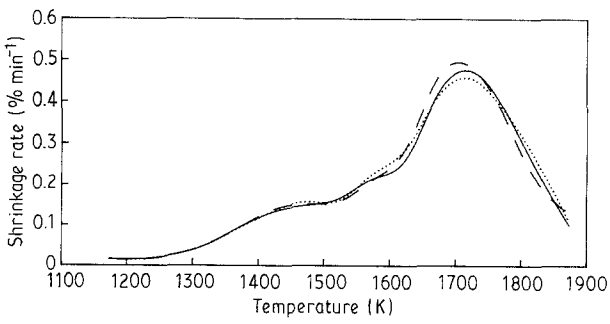

Figure 3 Shrinkage rate shown as a function of temperature during constant heating at 5 K min^{-1} for three replication experiments.

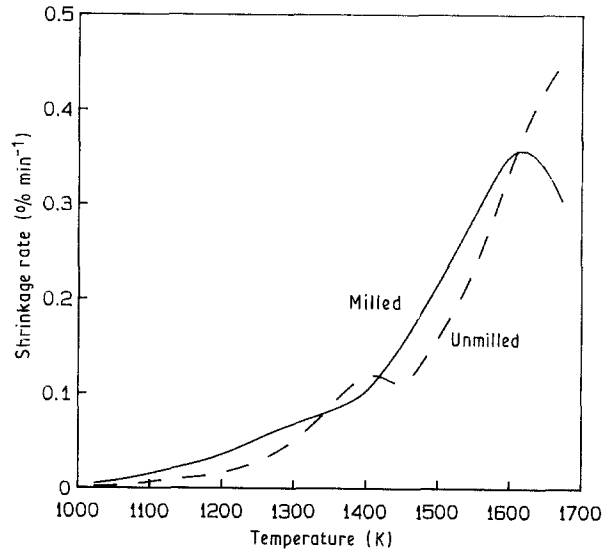

Figure 4 Shrinkage rate versus temperature plots for unmilled and milled alumina, showing the shrinkage rate peak change with the deagglomeration at heating rate of 5 K min^{-1}.

(to 20 p.p.m.) and iron (to 30 p.p.m.) contents. Fig. 4 provides a comparison of the shrinkage rate plots, showing that milling gave faster initial sintering and virtual elimination of the first peak near 1400 K. Note this peak is after the initial stage of sintering.

Measured shrinkages in the two test procedures were compared to determine if the weight of the pushrod was influencing the recorded shrinkages. The resulting values were essentially identical at temperatures below 1400 K. At higher temperatures the dilatometer shrinkage was larger. This may reflect the slight hot pressing effect from the pushrod contacting the specimen. The median pore size and grain size are shown versus the maximum temperature in Fig. 1c. There was an initial decrease in pore size (the green compact median pore size was 118 nm while the compact sintered at 1173 K had a pore size of 78 nm), followed by an increase at higher temperatures. In contrast, the grain size versus temperature indicates that significant grain growth did not occur until temperatures over approximately 1500 K.

4. Discussion

In the classic approach to sintering studies, it is assumed there is a single dominant mechanism. In this

regard, the surface area reduction results were analysed by the technique of German [23], in which a generalized kinetic expression was derived to relate surface area reduction to the sintering temperature during constant heating. The model is valid for approximately the first 50% surface area loss before growing inter-particle necks impinge or grain growth becomes significant. According to this model, the slope of Fig. 5 provides a measure of the ratio Q/γ, where Q is the activation energy and γ is related to the sintering mechanism. Application of this technique to the current experiments involves several assumptions, the most important of which is that a single mechanism was operative during sintering. This proved to be invalid and demonstrated the errors obtained with an Arrhenius analysis of single measures of sintering.

The calculated ratios of Q/γ are shown in Table II. The average value from the slope of Fig. 5 is 120 kJ mol^{-1}. For each sintering mechanism there exists recognized literature values of the activation energy and mechanism constant γ [38]. The candidate ratio values are based on the selections by Frost and Ashby [39], in which they used the lattice diffusion activation energy from Paladino and Kingery [40], the grain boundary diffusion activation energy from Cannon and Coble [41], and the surface diffusion activation energy of Robertson and Ekstrom [42]. From this selection process, it is evident that the best match between the measured and calculated Q/γ values is for grain boundary diffusion.

The shrinkages measured using dilatometry were analysed by a technique similar to that described by Young and Cutler [32]. In this procedure the shrinkage ($\Delta L/L_0$) during constant heating is plotted as ln ($\Delta L/L_0$) versus $1/T$ (Fig. 6). The slope of the straight line portion is $-Q/nR$ where Q is the activation energy for the shrinkage process, n depends on the mechanism, and R is the gas constant. As shown in Table II, the least squares fit to the results give a value of Q/n equal to 144 kJ mol^{-1}. This result is in best agreement with the predictions for grain boundary diffusion using the activation energy of 418 kJ mol^{-1} of Cannon and Coble [41] and a shrinkage mechanism n value of 3, giving a Q/n value of 139 kJ mol^{-1}. It is in agreement with the activation energy for grain boundary diffusion (440 kJ mol^{-1}) measured in constant heating rate experiments by Wang and Raj [43].

The fact that two separate sintering measures indicated dominance by the same mechanism would seem to indicate that grain boundary diffusion was the only operating mechanism during the sintering of this alumina powder. However, only rarely is one mechanism active and the more typical case is simultaneous

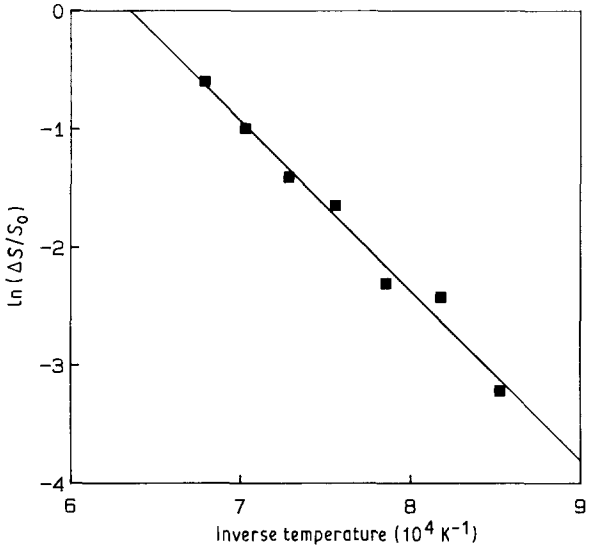

Figure 5 Surface area reduction data plotted against inverse temperature as a basis for extracting the apparent activation energy for surface area loss at heating rate of 5 K min^{-1}.

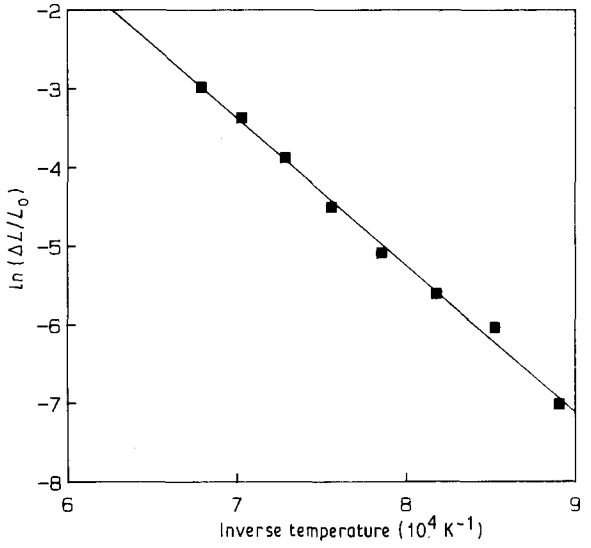

Figure 6 Shrinkage data treated on an Arrhenius plot as the basis for extracting the apparent activation energy at heating rate of 5 K min^{-1}.

TABLE II Surface area reduction and shrinkage activation energy analysis

Mechanism	γ	Q (kJ mol^{-1})	Q/γ (kJ mol^{-1})	Reference
Measured surface area Arrhenius slope, Q/γ = 120 kJ mol^{-1}				
Volume diffusion	2.7	447	177	35
Grain boundary diffusion	3.3	418	127	36
Surface diffusion	3.6	536	149	37
Measured shrinkage Arrhenius slope, Q/n = 144 kJ mol^{-1}				
Volume diffusion	2.5	447	191	35
Grain boundary diffusion	3.0	418	139	36

mechanisms. To gauge the relative possibility of simultaneous coarsening and densification mechanisms, Fig. 7 plots the measured initial stage surface area reduction versus shrinkage, and compares the results with the predictions for pure grain boundary diffusion and pure surface diffusion [22]. For the grain boundary diffusion case, the particle packing coordination is estimated at 4, based on the initial packing density used in this study [44]. The measured surface area reduction with shrinkage is much larger than that predicted if grain boundary diffusion was the only sintering mechanism. This indicates that surface diffusion is active during sintering of this powder, since this will contribute to surface area loss without causing additional shrinkage. The porosimetry results also indicate the action of surface diffusion since the median pore size increases from 76 nm at 1173 K to 108 nm at 1423 K, as the total porosity decreases. Similar behaviour has been reported during the initial stage of sintering for several systems [45].

Two computer simulations of initial stage sintering were employed to examine the possible sintering behaviour from simultaneous surface and grain boundary diffusion [2, 46]. As with other simulations, the programs operate using a data file containing the relevant material and process parameters as listed in Table III [39]. The first program, based on Ashby [47, 48], was used to determine the sintering map which shows the dominant sintering mechanism for various neck sizes and temperature combinations. It indicated that both grain boundary and surface diffusion should dominate the sintering of this alumina powder. The calculation predicts that surface diffusion will be the significant mechanism at the smaller neck sizes typical to initial stage sintering. This result differs from that attained through the analysis outlined in Table II, indicating that the actual sintering behaviour is more complex than sensed through an Arrhenius analysis of the apparent activation energy.

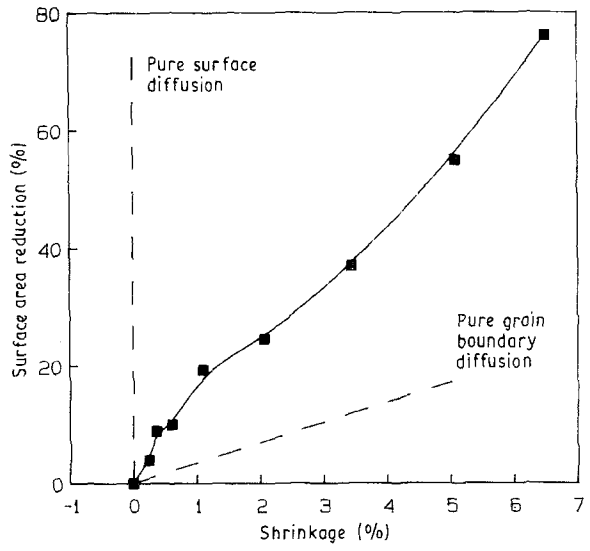

Figure 7 Surface area reduction against shrinkage during initial stage constant heating rate sintering of alumina. The observed behaviour is intermediate between the expectations based on pure surface diffusion and pure grain boundary diffusion.

TABLE III Material constants for computer simulations

Particle diameter: 0.14 μm
Melting temperature: 2318 K
Theoretical density: 3.97 $Mg\,m^{-3}$
Atomic volume: $2.11 \times 10^{-29}\,m^3$
Initial density: 1.35 $Mg\,m^{-3}$
Surface energy: 1.0 $J\,m^{-2}$
Pre-exponential for vapour pressure: 3.0×10^5 MPa
Activation energy for evaporation: 837 $kJ\,mol^{-1}$
Frequency factor for surface diffusion times surface thickness: $2.5 \times 10^{-6}\,m^3\,s^{-1}$
Activation energy for surface diffusion: 536 $kJ\,mol^{-1}$
Frequency factor for volume diffusion: $2.8 \times 10^{-3}\,m^2\,s^{-1}$
Activation energy for volume diffusion: 477 $kJ\,mol^{-1}$
Frequency factor for grain boundary diffusion times grain boundary width: $8.6 \times 10^{-10}\,m^3\,s^{-1}$
Activation energy for grain boundary diffusion: 418 $kJ\,mol^{-1}$

The second computer simulation is based on Johnson [5, 49]. It provides a basis for quantitatively predicting the surface area reduction and the shrinkage during initial stage sintering. Furthermore, this simulation allows for nonisothermal cycles such as the ones employed in this research. Using the material and process parameters from Table III, the simulated shrinkage and surface area results were greater than those determined by experiment. For example, the predicted shrinkage at 1273 K was 5.4% as compared with the measured value of 0.6%. As a result, computer experiments were conducted using variations in the activation energies of surface and grain boundary diffusion, since the simulation was most sensitive to these parameters. These values also seemed to be the most varied in the literature. The resulting simulated shrinkage and surface area reduction predictions were compared with the experimental values. The best fit to the experimental results required activation energies for surface diffusion Q_s and grain boundary diffusion Q_b of approximately 508 and 440 $kJ\,mol^{-1}$, respectively. Fig. 8 illustrates the sensitivity of the computer simulations to the input activation energy pairs Q_s and Q_b. It shows the initial stage shrinkage as measured by the dilatometer and the various computer simulated curves as the activation energy pair was varied. Fig. 9 gives the corresponding comparison of shrinkage rate between the measured values for milled and unmilled powders and the computer simulated values for the 508/440 $kJ\,mol^{-1}$ activation energy pair. The simulated curve is reasonably close to the experimental determinations. A comparison of the measured surface area reduction with that predicted from the computer simulation is given in Fig. 10. In comparison with shrinkage, the surface area reduction was less sensitive to variations in the activation energies. Fig. 11 shows a plot of simulated and experimental surface area reduction versus shrinkage. The simulation indicates the initial stage of sintering ended at approximately 3% shrinkage. Since the simulation does not include the effect of new contact formation that would occur with densification, the simulated surface area reduction is slightly less than the measured value, especially at the larger shrinkages. This is evident in Fig. 11. Using the 508/440 $kJ\,mol^{-1}$ activation energy pair, Fig. 12

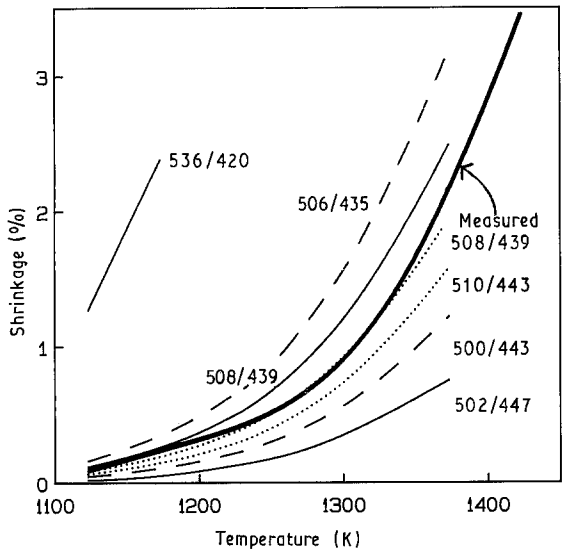

Figure 8 Computer simulated shrinkage versus temperature for various combinations of the activation energies for surface diffusion and grain boundary diffusion, Q_s/Q_b. The observed behaviour, shown as the bold curve, is best fitted by $Q_s = 508\ kJ\ mol^{-1}$ and $Q_b = 440\ kJ\ mol^{-1}$.

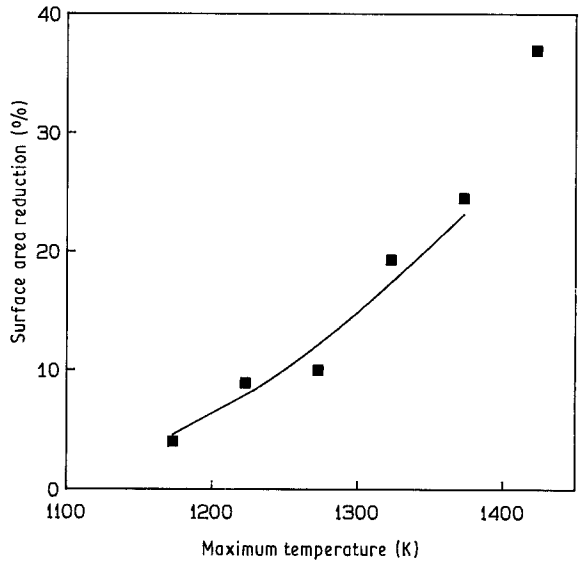

Figure 10 Computer simulated (——) surface area reduction versus temperature as compared with the measured (■) values (Q_s/Q_b = 508/440 kJ mol^{-1}) at heating rate of 5 K min^{-1}.

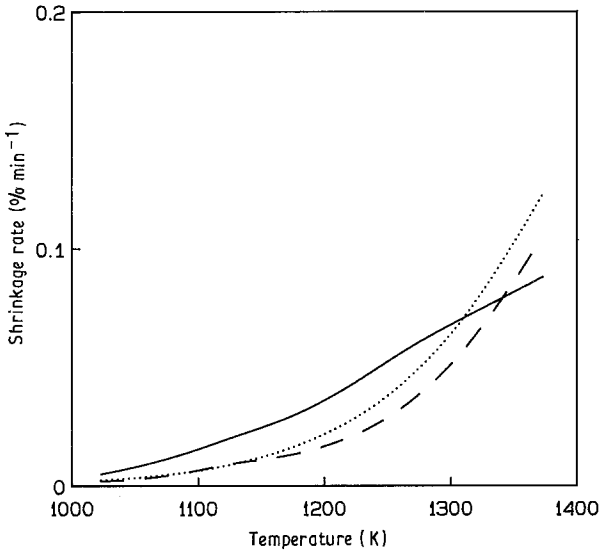

Figure 9 Computer simulated (· · ·) shrinkage rate versus temperature behaviour with the experimental results for milled (——) and unmilled (– – –) alumina powders using Q_s/Q_b = 508/440 kJ mol^{-1} at heating rate of 5 K min^{-1}.

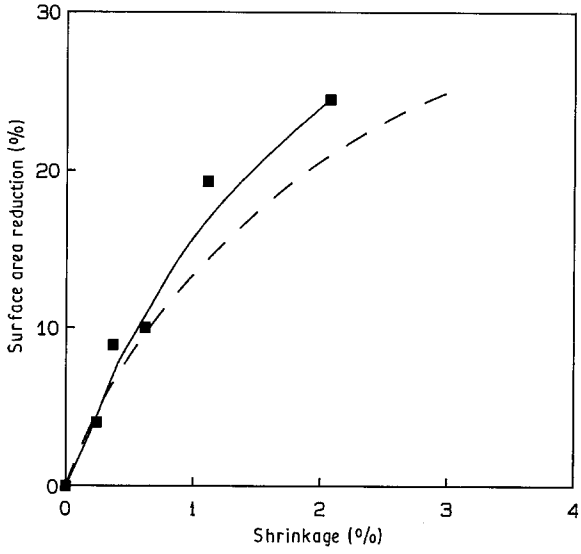

Figure 11 Simulated (– – –) and measured (——) surface area reduction versus shrinkage for constant heating at 5 K min^{-1}.

shows the computed relative neck growth rates by surface diffusion and grain boundary diffusion during sintering with a constant heating rate of 5 K min^{-1}. Surface diffusion dominates over the entire initial stage with grain boundary diffusion reaching approximately a 17% contribution late in the initial stage.

The above method for determining activation energies is unique in that it allows consideration of more than one transport mechanism with continual interactions during heating. The computer simulations showed that when the diffusion activation energies were adjusted by just 10 kJ mol^{-1}, there was considerable shift in the predicted behaviour. Arrhenius plots that are used in most analyses of sintering data only allow for the operation of one mechanism. This leads to inaccuracies when more than one mechanism is operating. Such behaviour is demonstrated by analysis of the computer simulated results using the techniques outlined in Figs 5 and 6. The resulting slope of the $\ln(\Delta L/L_0)$ versus $1/T$ plot gives an estimated grain boundary diffusion activation energy of 480 kJ mol^{-1}. Likewise, for surface area reduction the calculated activation energy is 390 kJ mol^{-1} assuming surface diffusion, or 315 kJ mol^{-1} assuming grain boundary diffusion. Note that these values from Arrhenius plots of the simulation results do not agree with the input simulation activation energy values of 440 and 508 kJ mol^{-1} for grain boundary and surface diffusion. Similar behaviour has been noted in other computer simulations, casting doubt on the accuracy of

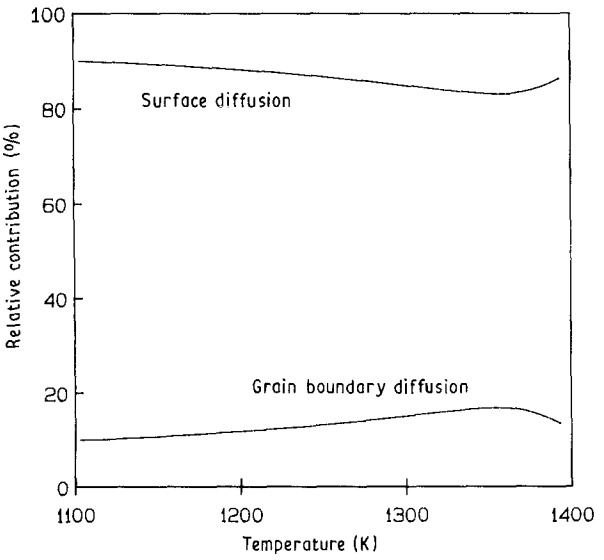

Figure 12 The relative contributions to the sintering neck growth process versus temperature. Surface diffusion is the dominant sintering process in the initial stage sintering of this submicron alumina when heated at 5 K min^{-1}.

apparent activation energies derived from shrinkage measurements [46]. This indicates that the use of sintering data as a basis for determining activation energies via Arrhenius plots is suspicious, especially if there are multiple sintering mechanisms and heating transients [12, 46].

Past assessments of surface and grain boundary diffusion behaviour for alumina are widely scattered. With an activation energy of 508 kJ mol^{-1}, the predicted surface diffusion coefficients are in reasonable agreement with several prior reports [21, 42, 50, 51], particularly with the determinations of Yen and Coble [50]. Grain boundary diffusivity in alumina is uncertain [13, 39, 41, 52–54]. The diffusivities based on the value of 440 kJ mol^{-1} determined in this study are in agreement with the prior reports by Cannon and Coble [41] and Wang and Raj [43]. In assessing the diffusivities, the pre-exponential factors were held constant. Changes in these factors would also affect the diffusion rates but this is a secondary effect in comparison with the dominant role of the activation energy.

The technique of simultaneous determination of two independent parameters during constant heating rate sintering provides a perspective on the densification and coarsening steps associated with sintering this submicron alumina powder. The technique illustrates the sensitivity of sintering behaviour to the diffusion activation energies. This analysis has demonstrated that multiple, independent measures of sintering are needed to understand the initial stage events. Traditional approaches to sintering do not deal with the possible interactions but typically assume one dominant process. The multiple measures of shrinkage, surface area reduction, pore size, and grain size provide insight as to the process. These results indicate the multiple mechanisms responsible for the initial stage sintering of alumina. Surface diffusion and grain boundary diffusion operate simultaneously in the initial stage. Even in the traditional high temperature isothermal sintering studies, it is highly probable that considerable surface diffusion occurs during heating.

5. Conclusions

Surface diffusion and grain boundary diffusion contribute simultaneously to the initial stage sintering of alumina. For the submicron powder used in these experiments, surface diffusion is responsible for most of the neck growth in the initial stage. The activation energies for these two diffusional processes are estimated at 508 and 440 kJ mol^{-1}, respectively, for surface and grain boundary diffusion. Constant heating rate experiments provide a successful basis for the isolation of the sintering response through the two independent measures of surface area reduction and shrinkage. This approach avoids the need for corrections associated with transient heating events before isothermal conditions are attained.

A common means of determining the apparent activation energy relies on an Arrhenius plot of a single sintering parameter such as shrinkage. Such an approach is error prone when sintering occurs by the action of two or more simultaneous transport mechanisms. Many of the previous studies dealing with the sintering of alumina assumed a single mechanism. This research demonstrates that activation energies from single measures of sintering are complicated, especially under conditions where two processes occur at the same time. Supplemental information is required on the basic microstructural transformation. A more appropriate analysis is based on simultaneous fits to independent sintering parameters like shrinkage and surface area.

Acknowledgements

Funding for this research was provided by fellowships for Sandra Hillman from Rensselaer and IBM, a research grant from the Basic Science Division of the Department of Energy, and equipment grants from the National Science Foundation.

References

1. H. E. EXNER, *Revs. Powder Met. Phys. Ceram.* **1** (1979) 7.
2. K. S. HWANG and R. M. GERMAN, in "Sintering and heterogeneous catalysis", edited by G. C. Kuczynski, A. E. Miller and G. A. Sargent (Plenum Press, New York, NY, 1984) p. 35.
3. F. A. NICHOLS and W. W. MULLINS, *J. Appl. Phys.* **36** (1965) 1826.
4. R. M. GERMAN and J. F. LATHROP, *J. Mater. Sci.* **13** (1978) 921.
5. D. L. JOHNSON, *J. Appl. Phys.* **40** (1969) 192.
6. H. E. EXNER and P. BROSS, *Acta Met.* **27** (1979) 1007.
7. P. BROSS and H. E. EXNER, *ibid.* **27** (1979) 1013.
8. J. W. ROSS, W. A. MILLER and G. C. WEATHERLY, *Z. Metallkde.* **73** (1982) 391.
9. K. BREITKREUTZ and D. AMTHOR, *Metall.* **29** (1975) 990.
10. R. M. GERMAN, *Scripta Met.* **14** (1980) 955.
11. H. E. EXNER, in "Sintering '87", Vol. 1, edited by S. Somiya, M. Shimada, M. Yoshimura and R. Watanabe (Elsevier, London, 1988) p. 291.

12. R. M. GERMAN, *Powder Met.* **22** (1979) 29.
13. D. L. JOHNSON and I. B. CUTLER, *J. Amer. Ceram. Soc.* **46** (1963) 545.
14. K. ASAGA and K. HAMANO, *Yogyo-Kyokai-Shi* **83** (1975) 40.
15. D. L. JOHNSON, in "Kinetics of reactions in ionic systems", edited by T. J. Gray and V. D. Frechette (Plenum Press, New York, NY, 1969) p. 331.
16. W. R. RAO and I. B. CUTLER, *J. Amer. Ceram. Soc.* **56** (1973) 588.
17. *Idem., ibid.* **55** (1972) 170.
18. R. L. COBLE, *ibid.* **41** (1958) 55.
19. T. L. WILSON and P. G. SHEWMON, *Trans. TMS-AIME* **236** (1966) 48.
20. C. GRESKOVICH and K. W. LAY, *J. Amer. Ceram. Soc.* **55** (1972) 142.
21. S. PROCHAZKA and R. L. COBLE, *Phys. Sintering* **2** [2] (1970) 15.
22. R. M. GERMAN and Z. A. MUNIR, in "Sintering and catalysis", edited by G. C. Kuczynski (Plenum Press, New York, NY, 1975) p. 259.
23. R. M. GERMAN, *Powder Tech.* **17** (1977) 287.
24. R. F. WALKER, *J. Amer. Ceram. Soc.* **38** (1955) 187.
25. G. C. KUCZYNSKI, L. ABERNETHY and J. ALLEN, in "Kinetics of high temperatures processes", edited by W. D. Kingery (John Wiley, New York, NY, 1959) p. 163.
26. R. L. COBLE, *J. Amer. Ceram. Soc.* **45** (1962) 123.
27. F. W. DYNYS and J. W. HALLORAN, *ibid.* **67** (1984) 596.
28. E. L. KEMER and D. L. JOHNSON, *Ceramic Bull.* **64** (1985) 1132.
29. J. P. SMITH and G. L. MESSING, *J. Amer. Ceram. Soc.* **67** (1984) 238.
30. T. S. YEH and M. D. SACKS, *ibid.* **71** (1988) 841.
31. J. ZHENG and J. S. REED, *ibid.* **72** (1988) 810.
32. W. S. YOUNG and I. B. CUTLER, *ibid.* **53** (1970) 659.
33. J. L. WOOLFREY and M. J. BANNISTER, *ibid.* **55** (1972) 390.
34. J. J. BACMANN and G. CIZERON, *ibid.* **51** (1968) 209.
35. T. S. WEI and R. M. GERMAN, in "Modern developments in powder metallurgy", Vol. 15, edited by E. N. Aqua and C. I. Whitman (Metal Powder Industries Federation, Princeton, NJ, 1985) p. 307.
36. D. B. CULLITY, in "Elements of X-ray diffraction" (Addison-Wesley, Reading, MA, 1978) p. 102.
37. T. S. WEI, PhD Thesis, Rensselaer Polytechnic Institute, Troy, NY (1987).
38. R. M. GERMAN and Z. A. MUNIR, *J. Amer. Ceram. Soc.* **59** (1976) 379.
39. H. J. FROST and M. F. ASHBY, in "Deformation-mechanism maps" (Pergamon Press, Oxford, UK, 1982) p. 98.
40. A. E. PALADINO and W. D. KINGERY, *J. Chem. Phys.* **37** (1962) 957.
41. R. M. CANNON and R. L. COBLE, in "Deformation of ceramic materials" (Plenum Press, New York, NY, 1975) p. 61.
42. W. M. ROBERTSON and F. E. EKSTROM, in "Kinetics of reactions in ionic systems", edited by T. J. Gray and V. D. Frechette (Plenum Press, New York, NY, 1969) p. 273.
43. J. WANG and R. RAJ, *J. Amer. Ceram. Soc.* **73** (1990) 1172.
44. R. M. GERMAN, in "Particle Packing Characteristics" (Metal Powder Industries Federation, Princeton, NJ, 1988) p. 90.
45. O. J. WHITTEMORE and J. A. VARELA, in "Sintering Processes", edited by G. C. Kuczynski (Plenum Press, New York, NY, 1980) p. 51.
46. K. S. HWANG, PhD Thesis, Rensselaer Polytechnic Institute, Troy, NY (1984).
47. M. F. ASHBY, *Acta Met.* **22** (1974) 275.
48. F. B. SWINKELS and M. F. ASHBY, *ibid.* **29** (1981) 259.
49. L. L. BERRIN and D. L. JOHNSON, in "Sintering and related phenomena", edited by G. C. Kuczynski, N. A. Hooton and C. F. Gibbon (Gordon and Breach, New York, NY, 1967) p. 369.
50. C. F. YEN and R. L. COBLE, *J. Amer. Ceram. Soc.* **55** (1972) 187.
51. T. MARUYAMA and W. KOMATSU, *ibid.* **58** (1975) 338.
52. K. KITAZAWA and R. L. COBLE, *ibid.* **51** (1974) 250.
53. S. I. WARSHAW and F. H. NORTON, *ibid.* **45** (1962) 479.
54. Y. OISHI and W. D. KINGERY, *J. Chem. Phys.* **33** (1960) 480.

Received 27 June 1990
and accepted 31 January 1991